Robust p53 Recovery Using Chattering Free Sliding Mode Control and a Gain-Scheduled Modified Utkin Observer

Article *in* Journal of Theoretical Biology · September 2021

DOI: 10.1016/j.jtbi.2021.110914

CITATIONS
4

READS
61

5 authors, including:

Rizwan Azam
COMSATS University Islamabad
13 PUBLICATIONS **79** CITATIONS
SEE PROFILE

Ali Arshad
COMSATS University Islamabad
39 PUBLICATIONS **364** CITATIONS
SEE PROFILE

Syed Bilal Javed
National Engineering & Scientific Commission, Islamabad, Pakistan
11 PUBLICATIONS **47** CITATIONS
SEE PROFILE

Aamer Iqbal Bhatti
University of Engineering & Technology Lahore
245 PUBLICATIONS **2,091** CITATIONS
SEE PROFILE

Robust p53 Recovery Using Chattering Free Sliding Mode Control and a Gain-Scheduled Modified Utkin Observer

Sheher Bano[a], Muhammad Rizwan Azam[a,*], Ali Arshad Uppal[a], Syed Bilal Javed[a], Aamer Iqbal Bhatti[b]

[a]*Department of Electrical Engineering, COMSATS University Islamabad, Pakistan*
[b]*Department of Electronics Engineering, Capital University of Science & Technology, Islamabad, Pakistan*

Abstract

p53 protein plays an essential role in protecting the genomic integrity of mammalian cells. A drastic decrease in the amount of p53 protein has been observed in cancerous cells. By using Nutlin-based small molecule drugs, the concentration of p53 can be restored to the desired level. This paper presents the drug-dosage design for p53 pathway, based on a control-oriented nonlinear model. A chattering free sliding mode control (CFSMC) strategy is employed to track the desired trajectory of p53 concentration for both of its dynamic behaviors, i.e., sustained and oscillatory responses. A gain-scheduled modified Utkin observer (GSMUO) is designed for robust state reconstruction and disturbance estimation. The simulation results show that CFSMC and GSMUO exhibit desired robustness and performance properties in the presence of parametric variations, an input disturbance and measurement noise. Moreover, a comprehensive simulation study, along with a detailed quantitative analysis is performed to compare CFSMC-GSMUO with four different techniques: a sliding mode control (SMC) with an equivalent control based sliding mode observer (SMO) and GSMUO, respectively, and a dynamic sliding mode control (DSMC) with SMO and GSMUO, respectively. The analysis demonstrates that

*Corresponding author
Email address: rizwan.azam@comsats.edu.pk (Muhammad Rizwan Azam)

the tracking error and utilization of the control energy is the least in the case of CFSMC-GSMUO as compared to its counterparts.
Keywords: p53 recovery, cancer control, drug dosage design, targeted cancer therapy and sliding mode control.

---

1. INTRODUCTION

Cancer is one of the major health problems all over the globe, and is the second major cause of death [1]. The DNA damage is the primary cause of cancer that occurs because of the inactivation of tumor suppressing proteins [2]. The p53 protein is a cancer suppressor, which protects the cells from malignant transformations during the DNA damage, hence called "guardian of the genome" [3]. Moreover, in its wild-type form, p53 acts as a transcription factor for many genes involved in the repair of damaged DNA, senescence, apoptosis and cell cycle arrest [4].

In about 50 % of cancer cases, p53 protein is either inactivated or mutated [5]. Due to its critical role in the suppression of cancer cells, p53 has become a mainstream focus for research on anti-tumor drug development. Considering the primary role of p53 in the regulation of various cellular mechanisms, precise control of its level and activity within cells is quite essential. As its low level can allow cancer initiation and persistent high level can speed up the aging process (by excessive apoptosis) [6]. In normal conditions, the level of p53 concentration in the cell is low. This is accomplished by the E3 ubiquitin ligase protein, named as Murine double minute 2 (MDM2) . The MDM2 is considered as the primary negative regulator of p53 [7], which controls the concentration of p53 and limits its functionality as an anti-tumor. An increase in the level of p53 causes the transcription of MDM2 mRNA, consequently increasing the level of MDM2. As a result, an auto-regulatory feedback loop is established between MDM2 and p53 for mutual regulation [7, 8]. In most tumor cases, the MDM2 is overexpressed and promotes the degradation of p53. The low level of p53 prohibits the repair of damaged DNA, apoptosis and cell cycle arrest. Hence, reactivating the level

of p53 has become the foremost therapeutic strategy in the fight against cancer.

The most promising strategy to elevate the concentration level of p53 is by preventing the interaction of p53-MDM2. Consequently, the normal functionality of the cell could be restored [9]. The structure of p53 reveals that the binding interaction between MDM2 and p53 can be suppressed by small non-peptide molecules. Nutlin is one of these small molecules based drugs having great therapeutic potential in disrupting the MDM2-p53 binding to activate p53 [10]. The pre-clinical data assures that Nutlin can restore the required p53 level, and can inhibit the cancerous cell growth in a dose-dependent manner [7, 11].

1.1. Motivation

The conventional cancer treatment methods include surgery, radiotherapy and chemotherapy. The common shortcoming associated with all these methods is that they destroy healthy cells along with cancerous cells. In the literature, various control strategies have been devised to optimize the drug usage in chemotherapy [12–16]. However, recently the research trend is shifting towards drug dosage design at the cellular level instead of the macroscopic level. Fluorescence-tagged protein reveals the complex nonlinear dynamics displayed by p53 at the cellular level [17]. Experiments show that the cell fate information is encoded in the p53 dynamics. The response pattern of p53 directly depends upon the type and severity of DNA damage. In response to less extensive DNA damage or the damage caused by ionizing radiation (IR), p53 displays a series of oscillations with fixed amplitude and a consistent period of $\sim$ 6h. The oscillatory response of p53 leads to either the DNA repair or the cell cycle arrest [18]. However, in the case of critical DNA damage, or the damage caused by ultraviolet (UV) radiations, p53 exhibits a sustained response [19, 20]. The amplitude and width of this sustained response are proportional to the extent of DNA damage. Consequently, the sustained response of p53 leads to the permanent cell death [17]. The diversity of these dynamic responses presents a challenge to the drug dosage design for the cancerous cells.

1.2. Related work

In the literature, numerous mathematical models have been developed in pursuit of a better understanding of the oscillatory mechanism within the p53-MDM2 feedback loop. Moreover, these models provide a framework to schedule and optimize the drug dosage to obtain the desired response. To investigate the working mechanism of the p53 pathway, scientists have developed various mathematical models that are based on stochastic models, continuous and discrete-time differential equations and delayed differential equations [21]. The mathematical models presented by [22–24] use delayed time differential equations that have infinite dimensions and exhibit oscillatory behavior. The models proposed in [25, 26] are quite complex, as they are developed by using multiple feedback loops instead of time delays.

In the literature, various model-based control strategies are implemented for the activation of the p53 pathway. Rigatos et al. [27] used the first-principal based model to design a nonlinear control scheme. A nonlinear feedback controller based on flatness theory is designed to maintain the required level of p53. In this control scheme, unknown states are estimated through a derivative-free nonlinear Kalman filter. In [28], a nonlinear control-oriented p53 model is integrated with a physiological based kinetic (PBK) model of Nutlin. Using this integrated approach, a mechanism to revive p53 protein is derived by employing a simple proportional type control. In [29], a two-loop feedback control structure is proposed to maintain the required level of p53. Wherein the outer loop uses a Lyapunov redesign based control system, which shifts the equilibrium point of the cancer state to a healthy state. In [30], a nonlinear sliding mode controller (SMC) is designed to achieve the desired concentration of p53. The dynamic sliding mode controller (DSMC) is also designed to address the chattering and discontinuous control input issues. Furthermore, an equivalent control based reduced-order sliding mode observer (SMO) is designed to determine the non-measurable states of the system.

1.3. Gap analysis

The above mentioned control techniques have some significant limitations. The model used in [27] is relatively complex and also the applied control technique is not inherently robust. In [28, 29], the modeling uncertainties, external disturbances and measurement noise are not considered in the control design. Moreover, it is assumed that the entire state vector is measurable, which is not possible in the actual scenario. The controller designed in [30] employs an equivalent control based SMO, that yields noisy estimates of the unknown states. Therefore, the performance of the control system deteriorates. Furthermore, the tracking error also converges asymptotically. Hence, the objective of the proposed research work is to design a model-based robust control to overcome the aforesaid shortcomings.

1.4. Major contributions

In the current work, the mathematical model of [31] is adapted to design a chattering free sliding mode controller (CFSMC), cf. [32], to achieve the desired concentration for both the dynamic behaviors of p53, i.e., the constant levels and oscillatory variations. Along with the typical benefits of SMC, the CFSMC additionally offers finite-time convergence and chattering reduction. A robust extended gain-scheduled modified Utkin observer (GSMUO) is employed to estimate the non-measurable states of the system. Moreover, GSMUO is also used for disturbance estimation to improve the control performance. The robustness property of the proposed control strategy is evaluated by considering measurement noise, parametric uncertainties and the input disturbance simultaneously. Moreover, the number of uncertain parameters is increased in the current work as compared to [30]. Despite more uncertain parameters, the proposed control scheme yields better performance compared to the previous work.

The structure of the paper is as follows. The control-oriented nonlinear mathematical model of the p53 pathway is discussed section 2 . In sections 3 and 4, the CFMSC controller and GSMUO observer design are presented, respectively. Section 5 represents results and discussions and finally, the paper is

concluded in section 6.

2. Control oriented model of the p53 pathway

Hunziker et al. [31] proposed a model that considers a p53-MDM2 mRNA positive feedback loop and a p53-MDM2 negative feedback loop to capture the dynamics of p53 response. Fig. 1 represents the schematic model in which interaction between p53, MDM2, MDM2 mRNA and the drug Nutlin is presented.

The control affine representation of the nonlinear model can be written as

$$\dot{x} = f(x) + g(x)(u - \zeta), \tag{1}$$

where $x \in \Re^4$ is the state vector, $g, f \in \Re^4$ are smooth vector fields and u represents the control input (Nutlin), which is measured in mg/kg and ζ represents the matched input disturbance. The expressions for $f(x)$ and $g(x)$ are presented as

$$f(x) = \begin{bmatrix} \sigma_p - \alpha x_1 - k_f x_1 x_3 + k_b x_4 + \gamma x_4 \\ k_t x_1^2 - \beta x_2 \\ k_{t1} x_2 - k_f x_1 x_3 + k_b x_4 - \gamma x_3 \\ k_f x_1 x_3 - k_f x_4 - \delta x_4 - \gamma x_4 \end{bmatrix},$$

$$g^T(x) = \begin{bmatrix} 0 & 0 & -k_m x_3 & 0 \end{bmatrix},$$

and measurable states of the system are represented by the output vector y_m

$$y_m^T = \begin{bmatrix} x_1 & x_3 \end{bmatrix}. \tag{2}$$

The definitions of model parameters and state variables are given in Table. 1. The nominal values of the model parameters are adopted from [31], which are also elaborated in Table. 1

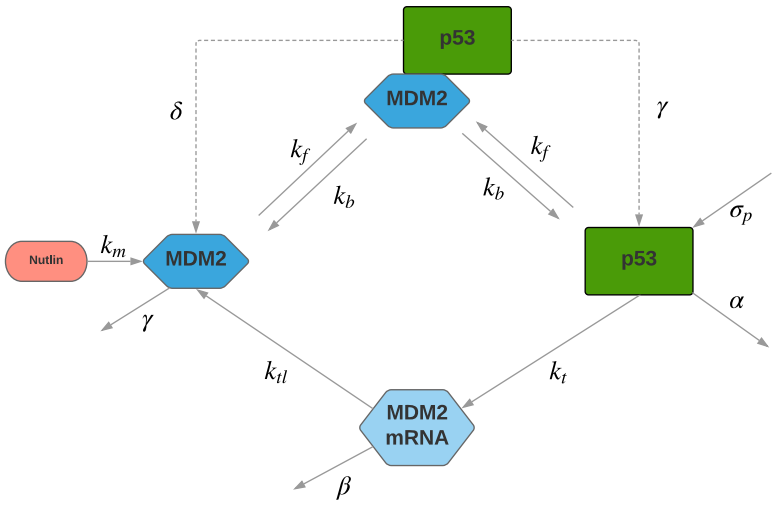

Figure 1: Schematic representation of p53 pathway dynamics [30].

symbol	**Description**	**Nominal Value**
x_1	Concentration of p53 protein [nM]	$--$
x_2	Mdm2 mRNA [nM]	$--$
x_3	Concentration of MDM2 protein [nM]	$--$
x_4	MDM2-p53 protein complex [nM]	$--$
α	Mdm2-independent degradation of p53 [hr^{-1}]	0.1
σ_p	p53 production rate [nMhr^{-1}]	1000
δ	Mdm2-dependent degradation of p53 [hr^{-1}]	11
k_t	Transcription of Mdm2 [1/nM/hr]	0.03
k_t1	Translation of Mdm2 [$--$]	1.4
β	Degradation of Mdm2 mRNA [$--$]	0.6
γ	Degradation of Mdm2 [$--$]	0.2
k_b	p53-Mdm2 dissociation [$--$]	7.2
$k_D = k_b/k_f$	p53-Mdm2 dissociation constant [nM]	1.44
k_m	Nutlin rate constant [hr^{-1}]	200

Table 1: Model parameters.

The objective of the controller design is to maintain the concentration of p53 at the desired level. Therefore, in the next section, the chattering free robust sliding mode controller (CFSMC) design is discussed for the p53 pathway.

3. Chattering free robust sliding mode controller design

In this section, a chattering free sliding mode controller (CFSMC) is designed to track the concentration of p53 at the desired level. As its name suggests, CFSMC eliminates chattering, which is the main issue in conventional sliding mode controllers [33–35]. Moreover, the sliding surface is designed in such a way that the tracking error converges in finite time. Furthermore, biological systems require a smooth control input, that can't be achieved in discontinuous SMC. Therefore, a systematic design of CFSMC is offered, which addresses the above mentioned problems of the conventional SMC [32].

Let $e = x_1 - x_{1d}$ is the tracking error between x_1 and its desired level x_{1d}. From the model in (1), it can be seen that the relative degree of e with respect to the control input u is 2. Therefore, twice differentiating e with respect to time results in the following error dynamics

$$\begin{aligned} \dot{e}_1 &= e_2, \\ \dot{e}_2 &= h(x,t) + b(x,t)u, \end{aligned} \tag{3}$$

where, the nonlinear functions $h(x,t)$ and $b(x,t)$ are characterized as

$$\begin{aligned} h(x,t) = e_2 + (\alpha + k_f x_3) + (k_b + \gamma)\dot{x}_4 - k_f k_{tl} x_1 x_2 + \ k_f^2 x_1^2 x_3 \\ - k_f(kb + \gamma)x_1 x_4 + kf\gamma x_1 x_3 - k_f k_m x_1 x_3 \zeta, \\ b(x,t) = k_f k_m x_1 x_3. \end{aligned}$$

In $h(x,t)$, ζ is the matched input disturbance. The disturbance profile should fulfill the following assumption:

Assumption: $||\zeta|| \leq \zeta_0, \zeta_0 \in \Re^+$ is a norm bounded input disturbance with a smooth and bounded time derivative, i.e. $\dot{\zeta} \leq \psi$, where $||\psi|| \leq \psi_0, \quad \psi_0 \in R+$

is a smooth function.

Now, to regulate e_1 and e_2 in finite time, a terminal sliding mode (TSM) manifold can be selected for the system in (3) as

$$s = \dot{e}_2 + c_2 \operatorname{sgn}(e_2)|e_2|^{r_2} + c_1 \operatorname{sgn}(e_1)|e_1|^{r_1}, \tag{4}$$

where c_i and r_i are design parameters.

The parameters c_1 and c_2 are selected in such a way that the polynomial $\rho^2 + c_2\rho + c_1$ corresponding to the system (4), is Hurwitz i.e., the roots of this polynomial lie in the open left half of the complex plane. In the above polynomial, ρ is the Laplace operator. The constants r_i can be determined based on the following conditions [36]

$$\begin{cases} r_1 = \vartheta \\ r_2 = \frac{2r_1}{1+r_1}, \end{cases} \tag{5}$$

where $\vartheta \in (1-\epsilon, 1), \epsilon \in (0,1)$. Selecting c_i and r_i in above fashion represents the establishment of the ideal sliding mode $s = 0$ for (3). The system can now converge to its equilibrium point, i.e. $e_1 = 0$ from any arbitrary initial condition along the sliding surface $s = 0$ in finite-time [37].

In order to reach $s = 0$ in finite-time, the control law is designed as

$$\begin{aligned} u &= \frac{1}{k_f k_m x_1 x_3}(u_1 + u_2), \\ u_1 &= -h(x,t) - c_2 \operatorname{sgn}(e_2)|e_2|^{r_2} - c_1 \operatorname{sgn}(e_1)|e_1|^{r_1}, \\ \dot{u}_2 &= -Tu_2 - \upsilon \operatorname{sgn}(s), \end{aligned} \tag{6}$$

where T and υ are positive constants. From (6) it can be seen that u is continuous as the only discontinuity is included in the derivative of u_2.

3.1. Existence of Sliding Mode

Consider a positive definite Lyapunov function in order to prove the existence of sliding mode

$$V(x,t) = \frac{1}{2}s^2 > 0, \tag{7}$$

with the time derivative given as

$$\dot{V}(x,t) = s\,\dot{s}, \tag{8}$$

by using (4) and (3) s can be written as

$$s = h(x,t) + u_1 + u_2 + c_1 sign(e_1)|e_1|^{r_1} + c_2 sign(e_2)|e_2|^{r_2}. \tag{9}$$

By substituting expression for u_1 in (9), $s = u_2$ and $\dot{V}$ becomes

$$\begin{aligned} \dot{V} &= s(-Tu_2 - v sign(s)), \\ &= -|s|(T|s| + v), \\ &\leq -v|s| < 0. \end{aligned} \tag{10}$$

From the above expression it is evident that the system (3) will reach to $s = 0$ in finite time.

3.2. Zero Dynamics

After establishment of the sliding mode, i.e. $s = 0$ at $t = t_0$, it is mandatory to evaluate the stability of the zero dynamics. When sliding mode is enforced both e_1 and e_2 in (3) converge to the origin, which implies $x_1 \rightarrow x_{1d}$ and $\dot{x}_1 \rightarrow \dot{x}_{1d}$. As the tracking error has a relative degree 2 with respect to the control input, and the order of the system in (1) is 4, therefore, the zero dynamics is of the second order and is comprised of

$$\dot{x_2} = -\beta x_2 + k_t x_{1d}^2, \tag{11}$$

$$\dot{x_4} = k_f x_1 x_3 - (k_b + \delta + \gamma) x_4. \tag{12}$$

By substituting $k_f x_1 x_3$ from (1) into (12), $\dot{x}_4$ can be re-written as

$$\dot{x}_4 = -(k_f + \delta - k_b) x_4 + (\sigma_p - \alpha x_{1d} - \dot{x}_{1d}). \tag{13}$$

Now, (11) and (13) represent linear ODEs with constant and bounded inputs. These equations can be solved to yield

$$\begin{aligned} \tilde{x}_2(\tilde{t}) &= \tilde{x}_2(0) \exp\left(-\beta \tilde{t}\right) + \frac{k_t x_{1d}^2}{\beta}\Big\{1 - \exp\left(-\beta \tilde{t}\right)\Big\}, \\ \tilde{x}_4(\tilde{t}) &= \tilde{x}_4(0) \exp\left(-\Pi \tilde{t}\right) + \frac{\sigma_p - \alpha x_{1d} - \dot{x}_{1d}}{\Pi}\Big\{1 - \exp\left(-\Pi \tilde{t}\right)\Big\}, \end{aligned} \tag{14}$$

where $\Pi = k_f + \delta - k_b$ and $\tilde{t} = t - t_0$.

From Table. 1, it can be seen that both β and Π in (14) are positive, therefore, $\tilde{x}_2 \to k_t x_{1d}^2/\beta$ and $\tilde{x}_4 \to (\sigma_P - \alpha x_{1d} - \dot{x}_{1d})/\Pi$. Now, when $s = 0$, $x_1 \to x_{1d}$, $\dot{x}_1 \to \dot{x}_{1d}$, $x_2 \to \tilde{x}_2$ and $x_4 \to \tilde{x}_4$, therefore, the steady state value of x_3 can be found by algebraically solving $\dot{x}_1$ in (1) as

$$\tilde{x}_3 = \frac{1}{k_f x_{1d}} \Big(\sigma_p - \alpha x_{1d} + (k_b + \gamma)\tilde{x}_4 - \dot{x}_{1d} \Big). \tag{15}$$

Moreover, from (6), when $s = 0$, $u_2 \to 0$, so $u = u_1 = -h(\tilde{x}, \tilde{t})$. Therefore, during sliding mode the system states and the control law stay bounded: $x \to \tilde{x}$ and $u \to U \in \Re$, which shows that zero dynamics is stable and control design is valid.

The control law in (6) requires all the system sates, therefore, it is required to design an estimator to find the unknown states. Moreover, in order to improve the performance of the closed loop system, the disturbance ζ is also estimated. The design of the estimator is discussed in the subsequent section.

4. Extended Gain-Scheduled Modified Utkin Observer

In this section the design of an extended gain-scheduled Utkin observer (GSMUO) is presented. The observer yields robust state and disturbance estimation. As compared to the conventional sliding mode observers, GSMUO brings the sliding motion in finite time, cf. [38, 39].

In order to estimate the disturbance, an additional state is added in (1). Now, the state vector includes another state $x_5 = \zeta$ and the nonlinear function $f(x)$ can be re-written as

$$f(x) = \begin{bmatrix} \sigma_p - \alpha x_1 - k_f x_1 x_3 + k_b x_4 + \gamma x_4 \\ k_t x_1^2 - \beta x_2 \\ k_{t1} x_2 - k_f x_1 x_3 + k_b x_4 - \gamma x_3 + k_m x_3 x_5 \\ k_f x_1 x_3 - k_f x_4 - \delta x_4 - \gamma x_4 \\ 0 \end{bmatrix}. \tag{16}$$

According to [30], ζ varies very slowly with time, therefore, dynamics of ζ in the extended system is governed by $\dot{\zeta} = 0$.

The observer design is based on the quasi-linear decomposition (cf. [40]) of p53 pathway model given in (1). The decomposition depicts the true nonlinear dynamics of (1), such that

$$\dot{x} = f(x) + B(x)u = A(x)x + B(x)u, \tag{17}$$

where $A(x) \in R^{5\times 5}$ is given as

$$A(x) = \begin{bmatrix} | & | & | & | & | \\ a_1 & a_2 & a_3 & a_4 & a_5 \\ | & | & | & | & | \end{bmatrix},$$
$$a_i = \nabla f_i(x) \frac{f_i(x) - x^T \nabla f_i(x)}{x^T x}, x \neq 0,$$

where $\nabla f_i(x)$ is the gradient of the element i of the vector field $f(x)$ in the direction of x. The matrix $B(x) \in \Re^5$ is characterized as

$$B^T(x) = \begin{bmatrix} 0 & 0 & k_m x_3 & 0 & 0 \end{bmatrix}.$$

The first step in GSMUO design is to re-order the states of the system as

$$[z \quad y_m]^T = Tx, \tag{18}$$

where $z^T = [x_2 \quad x_3 \quad x_5]$ are the unknown states and y_m as given in 2 are measured states, and $T = [N_C \quad C^T]^T$ is the transformation matrix. The output matrix C can be obtained from 2, both C and its null space N_C are given as

$$C = \begin{bmatrix} 1 & 0 & 0 & 0 & 0 \\ 0 & 0 & 1 & 0 & 0 \end{bmatrix},$$
$$N_C^T = \begin{bmatrix} 0 & 1 & 0 & 0 & 0 \\ 0 & 0 & 0 & 1 & 0 \\ 0 & 0 & 0 & 0 & 1 \end{bmatrix}.$$

The transformed system can be represented as

$$\begin{bmatrix} \dot{z} \\ \dot{y}_m \end{bmatrix} = TA(x)T^{-1} \begin{bmatrix} z \\ y_m \end{bmatrix} + TB(x)\ u\ . \tag{19}$$

Now, the new system can be partitioned as

$$TA(x)T^{-1} = \left[\begin{array}{c:c} W_{11}(x) & W_{12}(x) \\ \hdashline W_{21}(x) & W_{22}(x) \end{array}\right], \quad TB(x) = \left[\begin{array}{c} b_1 \\ \hdashline b_2 \end{array}\right]. \tag{20}$$

The transformed system can be re-written as

$$\begin{aligned} \dot{z} &= W_{11}(x)z + W_{12}(x)y_m + b_1 u\ , \\ \dot{y}_m &= W_{21}(x)z + W_{22}(x)y_m + b_2 u\ . \end{aligned} \tag{21}$$

The structure of the corresponding GSMUO is specified as

$$\begin{aligned} \dot{\hat{z}} &= W_{11}(x)\hat{z} + W_{12}(x)\hat{y}_m + b_1 u + L\upsilon - G_1 e_y\ , \\ \dot{\hat{y}}_m &= W_{21}(x)\hat{z} + W_{22}(x)\hat{y}_m + b_2 u - \upsilon - G_2 e_y\ , \end{aligned} \tag{22}$$

where $\hat{z}$ and $\hat{y}_m$ are estimates of unknown states and measurements, respectively. The Luenberger-type gain matrices $G_1 \in \mathbb{R}^{3\times 2}$ and $G_2 \in \mathbb{R}^{2\times 2}$ provide robustness and $L \in \mathbb{R}^{3\times 2}$ is a feedback gain matrix. The discontinuous vector υ can be described as

$$\upsilon = \begin{bmatrix} M_1\ \mathrm{sgn}(\hat{y}_{m,1} - y_{m,1}) \\ M_2\ \mathrm{sgn}(\hat{y}_{m,2} - y_{m,2}) \end{bmatrix}, \tag{23}$$

with $M_1, M_2 \in R^+$. The nonlinear switching terms guarantee finite-time convergence. The error dynamics of the system can be expressed as

$$\dot{\hat{e}}_z = W_{11}(x)\hat{e}_z + W_{12}(x)\hat{e}_y + L\upsilon - G_1 e_y\ , \tag{24}$$

$$\dot{\hat{e}}_y = W_{21}(x)\hat{e}_z + W_{22}(x)\hat{e}_y - \upsilon - G_2 e_y, \tag{25}$$

where $e_z = \hat{z} - z$ and $e_y = \hat{y}_m - y_m$.

A new error variable $\bar{e}_z = e_z + L e_y$ is introduced and now the error dynamics can be redefined with respect to these error variables as

$$\left[\begin{array}{c} \dot{\bar{e}}_z \\ \hdashline \dot{e}_y \end{array}\right] = \left[\begin{array}{c:c} \bar{W}_{11}(x) & \bar{W}_{12}(x) \\ \hdashline W_{21}(x) & \bar{W}_{22}(x) \end{array}\right] \left[\begin{array}{c} \bar{e}_z \\ \hdashline e_y \end{array}\right] + \left[\begin{array}{c} \mathbf{0} \\ \hdashline -I \end{array}\right] \boldsymbol{\upsilon}, \tag{26}$$

with the sub-matrices defined as

$$\begin{aligned}
\bar{W}_{11} &= W_{11}(x) + L\, W_{21}(x)\ , \\
\bar{W}_{12} &= W_{12}(x) - \bar{W}_{11}L - G_1 + L\,(W_{22}(x) - G_2)\ , \\
\bar{W}_{22} &= W_{22}(x) - G_2 - W_{21}(x)\, L\ .
\end{aligned} \tag{27}$$

The result in (26) transforms the estimation problem to a stabilization problem in e_y and $\bar{e}_z$, where υ behaves like an auxiliary observer input. The discontinuous gains M_1 and M_2 in (23) are selected such that they satisfy the reaching condition $e_{y_i}\dot{e}_{y_i} < 0$, where e_{y_i} is the sliding variable. The reaching condition can be proved by taking the following Lyapunov function,

$$V_i = \frac{1}{2}e_{y_i}^2\ . \tag{28}$$

The time-derivative of (28) along with (26), yields

$$\begin{aligned}
\dot{V}_i &= e_{y_i}\left(W_{21_i}(x)\bar{e_z} + \bar{W}_{22_i}e_{y_i} - \upsilon_i\right)\ , \\
&\leq -|e_{y_i}|\left(M_i - |W_{21_{(i)}}(x)\bar{e_z} + \bar{W}_{22_{(i)}}e_{y_i}|\right)\ ,
\end{aligned} \tag{29}$$

where $W_{21_{(i)}}(x)$ and $\bar{W}_{22_{(i)}}$ represent the i^{th} row of matrices $W_{21}(x)$ and $\bar{W}_{22}$ respectively. Now if $M_i \geq \varsigma + |W_{21_{(i)}}(x)\bar{e_z} + \bar{W}_{22_{(i)}}e_{y_i}|$, where ς is positive constant, then

$$\dot{V}_i = -\sqrt{2V_i}\varsigma\ ,$$

and the measurement error converges to zero in finite-time [41], i.e., $e_{y_i} \to 0$ given by

$$t_s \leq \frac{\sqrt{2V_i(0)}}{\varsigma}\ .$$

The gain matrices L and G_2 are designed using linear quadratic regulator (LQR) method and are selected such that the matrices $W11(x) + LW21(x)$ and $W_{22}(x) - G_2 - W_{21}(x)\, L$ are Hurwitz. G_1 is selected such that $\bar{W}_{12} = W(x)_{12} - \bar{W}_{11}L - G_1 + L\,(W(x)_{22} - G_2) = 0$. The suitable choice of L, G_1 and G_2 ensure the state observation and asymptotic convergence of the error dynamics.

5. Results and Discussions

The complete control implementation scheme of the controller along with the observer is shown in Fig. 2. The measurement noise n is also introduced in the implementation.

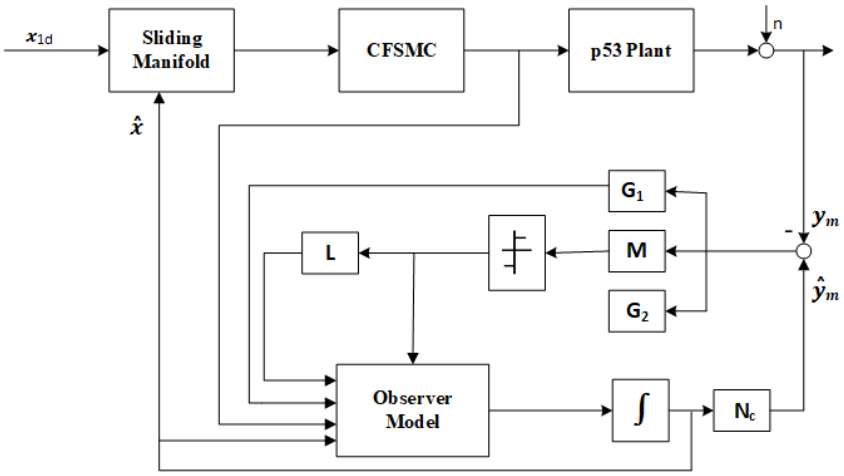

Figure 2: Control implementation scheme for the system

One of the major challenges in establishing the computer based models of a biological systems is the accurate measurement of the model parameters. Due to the differences in the in-vivo and in-vitro conditions, the in-vitro parameter estimation are usually imprecise. Moreover, the traditional parameter estimation techniques require a huge amount of data to accurately estimate the parameters for a wide range of operation. However, due to the time-consuming and expensive techniques of measurements, the availability of biological data is generally limited [7]. Therefore, the model parameters often contain uncertainties that should be taken care of while implementing the feedback control scheme. For the p53 pathway model presented in [30], some of the parameters presented in Table. 1 are fixed. However, the parameters k_f, δ, α, k_b, σ and γ can vary due to the dynamic environmental conditions, application of different stresses, and cell-cell variability. To inspect the robustness property of the proposed control technique, 20% variations are introduced in the nominal system param-

eters as illustrated in Table. 2. It is worth mentioning that the nominal system parameters are used in the controller and the estimator.

The time profile of disturbance is depicted in Fig. 3. The input disturbance models undesirable signals from neighboring cells, the effect of unintended cross-talk between pathways and environmental stresses on the amount of loss in the concentration of the drug Nutlin. As the exact function of disturbance can not be known, hence, a hypothetical time profile of the disturbance is assumed, as depicted in Fig. 3. The disturbance profile follows the standard drug concentration profile in the human body succeeding an oral delivery [42]. Moreover, it is assumed that the measurements of x_1 and x_3 from respective sensors are noisy. Hence, in each measured state, an additive white Gaussian noise (AWGN) with zero mean and a variance of 1×10^{-4} is also considered.

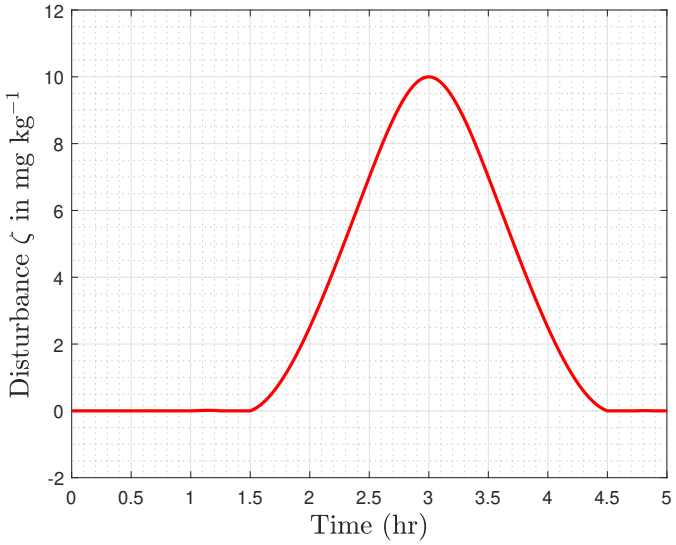

Figure 3: Time profile of the disturbance [30]

Table 2: Perturbed parametric values

parameter	**Nominal value**	**Perturbed value**
δ	11	13.2
γ	0.2	0.24
k_f	5.1428	6.168
α	0.1	0.12
k_b	7.2	8.44
σ_p	1000	1200

A detailed simulation analysis is performed in the following subsections to track the reference trajectories of the p53 protein. The effectiveness of the proposed control technique is tested for two separate cases. For the first test case scenario, the p53 protein displays a trajectory with three different levels. While for the second case, the concentration of p53 protein exhibits an oscillatory variation with a period of $\sim$ 6 hrs.

5.1. Case I: Sustained p53 Response

According to various research studies carried out on cancerous cells, it is acclaimed that the range of p53 (x_1) is 10-30 nM in normal healthy cells [31, 43]. While in the cancerous cells, the concentration of p53 protein is required to be around 400 nM [23, 44]. However, overexpression of MDM2 (x_3) prohibits p53 to raise its current level. In the simulations, x_1 is initialized from a low concentration level i.e., 17 nM [43]. The desired p53 concentration trajectory (obtained from [27]) is presented in Figure 4. The trajectory exhibits a piecewise constant variations and consists of three distinct levels. Tracking of such kind of trajectory guarantees that the proposed control system can track any desired concentration level of p53 protein during the treatment of cancer. It is worth mentioning that in the first 0.5 hours, the system is operated in the open-loop until the p53 approaches the desired level, then the controller starts working and the closed-loop operation strives to maintain the desired profile. It is pertinent

to mention that the observer is running during both the open-loop and the closed-loop operations of the system.

A comparison between conventional SMC, DSMC, and CFSMC along with SMO and GSMUO is presented, which are implemented to track the desired trajectory. Fig. 5 presents the output tracking performance of various control schemes. The GSMUO, along with the robust state estimation, also filters out the measurement noise introduced in the plant, hence, providing a smooth response. On the contrary, the outputs of the SMO based SMC and DSMC schemes are relatively noisy, as the measured states are being utilized in the controller design [30]. It can be seen that the best tracking behavior for output (p53) is obtained in the case of GSMUO based CFSMC. Due to finite time convergence of the tracking error, the response of CFSMC is the fastest as compared to its counterparts. This can be seen in the zoomed view of Fig. 5.

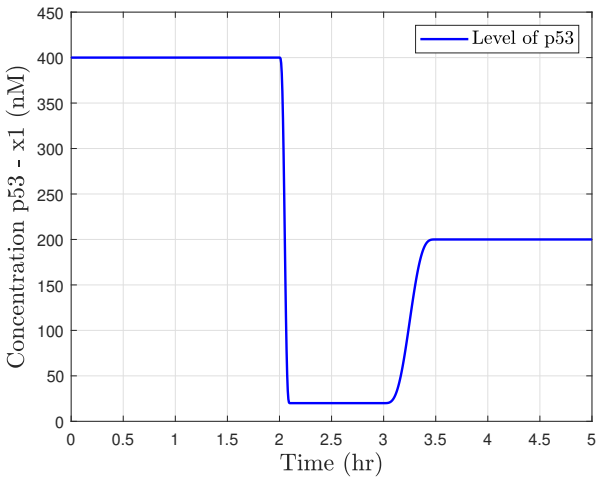

Figure 4: Desired trajectory for p53 protein

Fig. 6 shows the comparison of the control input (Nutlin) generated by SMC, DSMC and CFSMC. It is shown that the control effort for all control techniques remains under 90 mg/kg, which is well within the upper bound reported in the literature i.e., 200 mg/kg [45]. Fig. 7 shows the closed-loop tracking error of all

the implemented control techniques. As expected, the tracking error is the least in case of CFSMC. The sliding variable s, for CFSMC is shown in Fig. 8.

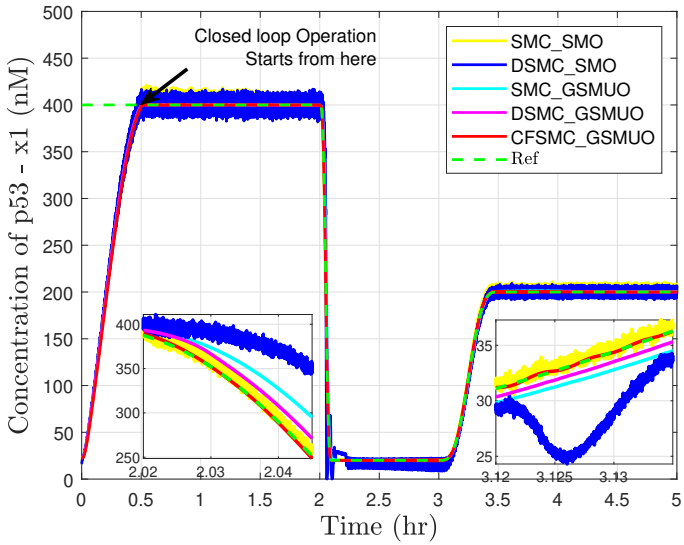

Figure 5: Concentration of p53 protein with time

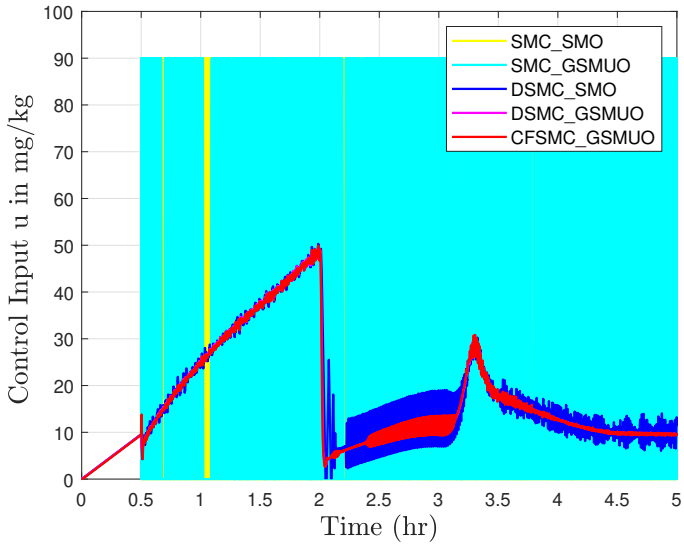

Figure 6: Control input with time

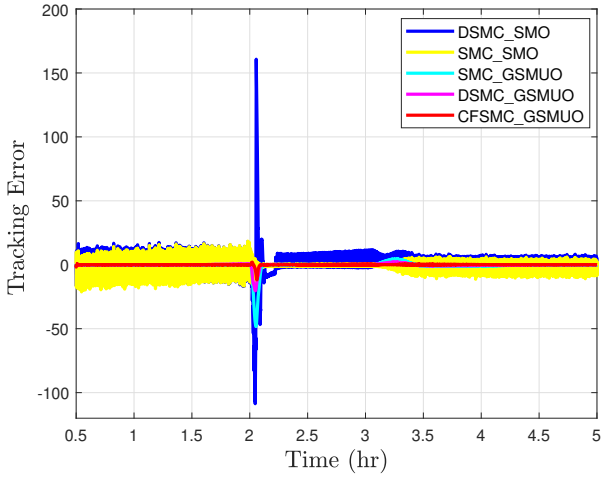

Figure 7: Closed loop tracking error with time

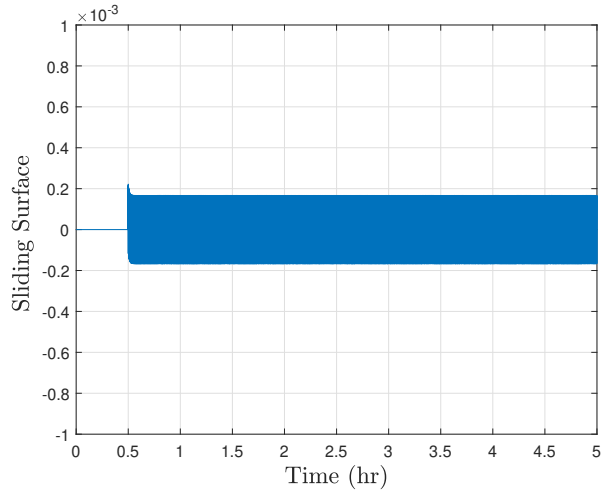

Figure 8: Sliding Surface for CFSMC

In order to assess and compare the effectiveness of the control strategies applied for test case I, a quantitative analysis is also carried out. The performance evaluating criteria for the comparison are the root mean squared tracking error ($RMSE$) and the average power of the control input. The formula for calculat-

ing the $RMSE$ is given as

$$RMSE = \sqrt{\frac{1}{N}\sum_{i=1}^{N} e^2(i)} \ , \ \ e(i) = x_1(i) - x_{1d}(i) \ , \tag{30}$$

where N represents the total number of samples. The average power (P_{avg}) of the control signal is computed using the following formula

$$P_{avg} = \frac{1}{N}\sum_{i=1}^{N} u^2(i) \ . \tag{31}$$

$RMSE$ and P_{avg} for all the control techniques are provided in Table 3. The comparison reveals that CFSMC based GSMUO has the best tracking performance and also lower control energy consumption.

Controller	**RMSE** (nM)	$\mathbf{P}_{\text{avg}}$ $(mg/kg)^2$
SMC-SMO	3.2939	1391.3
DSMC-SMO	10.1226	440.4466
DSMC-GSMUO	1.7597	425.8672
SMC-GSMUO	4.1408	819.1943
CFSMC-GSMUO	0.6694	422.9480

Table 3: RMSE and P_{avg} of five control techniques for three level trajectory

In order to investigate the estimation performance of the estimator, it is mandatory to initialize both the GSMUO and the plant with different initial conditions. The initial state vectors for the nonlinear plant and observer are chosen as $\boldsymbol{x}(0) = [17\ 14\ 8\ 91\ 0]^T$, and $\hat{\boldsymbol{x}}(0) = [23\ 24\ 12\ 80\ 0.1]^T$, respectively. The Figs. 9 and 10 represent the estimated states x_2 and x_4 of the reduced order SMO, cf. [30], and GSMUO. It is clear from the results that the performance of GSMUO is better as compare to SMO. Fig. 11 shows the estimation of disturbance which is considered as the third unknown state.

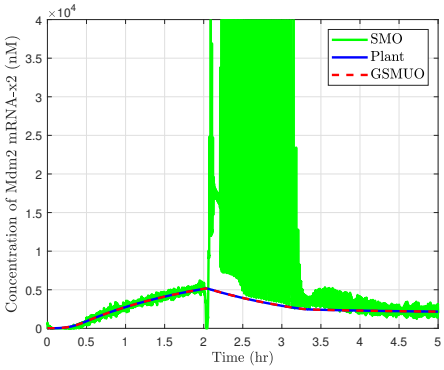

Figure 9: Concentration of Mdm2 mRNA-x_2

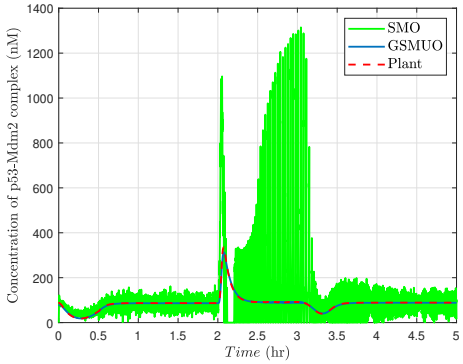

Figure 10: Concentration of p53-Mdm2 complex-x_4

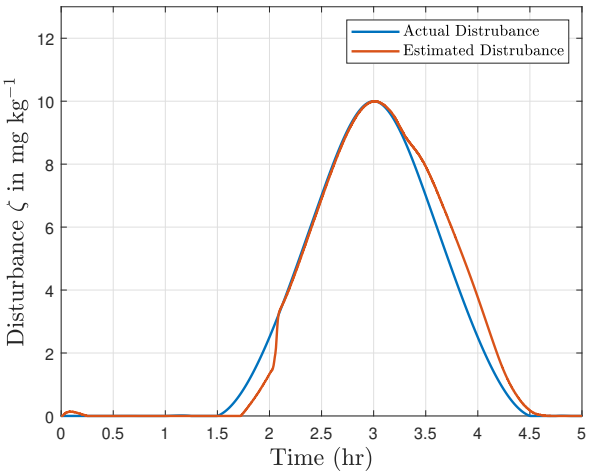

Figure 11: Estimation of disturbance

The best controller-observer pair (CFSMC-GSMUO) is employed for the oscillatory trajectory of case II, described in the subsequent section.

5.2. Case II: Oscillatory p53 Response

The simulation results for test case II are presented in Figs. 12 and 13. p53 shows the oscillatory response when the extent of DNA damage is not severe.

This type of response controls the growth of cancerous cells by cell cycle arrest. The period of oscillation is 4.5 to 6 hrs. Fig. 12 shows that the p53 concentration successfully tracks the desired sinusoidal trajectory taken from [27]. The value of x_1 is again initialized from a low level, i.e., 17nM. The simulation results of the proposed controller display a much better tracking response as compared to the results obtained in [27]. Figure 13 presents the control effort for test case II.

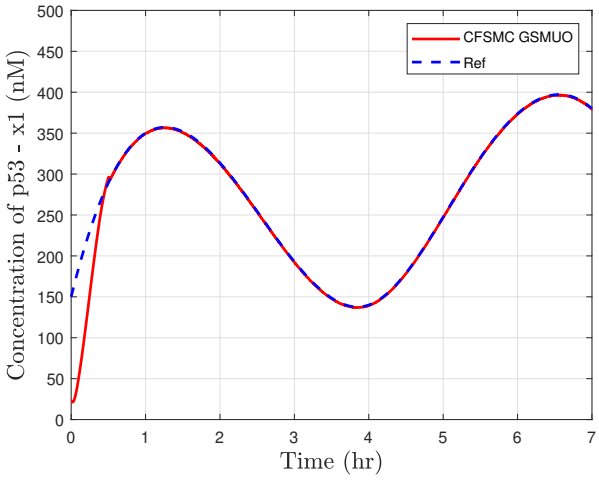

Figure 12: p53 oscillatory response

6. Conclusion

In this paper, a model-based CFSMC control is designed to achieve the desired concentration of p53 protein for two different test cases. In the first case, a sustained p53 response is tracked for three different levels, whereas, in the second case, tracking is achieved for an oscillatory p53 response. To maintain the desired levels of p53, the Nutlin drug is used as a control input. To make the feedback control design possible, the unknown states of the model are reconstructed with GSMUO. The boundedness of the zero dynamics is also demonstrated. A quantitative comparison between the controllers: SMC, DSMC and

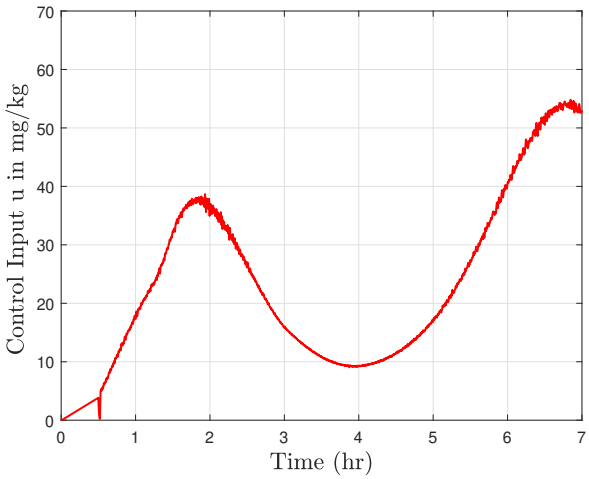

Figure 13: Controlled input for p53 oscillatory response

CFSMC and the observers: SMO and GSMUO is performed which shows that the CFSMC based GSMUO yields the least error and control energy. The proposed research work provides a model for the development of a p53-based regulatory strategy and can assist in targeted cell therapy.

References

[1] H. Nagai, Y. H. Kim, Cancer prevention from the perspective of global cancer burden patterns, Journal of thoracic disease 9 (2017) 448.

[2] S. A. Goffin, Targeting the p53/MDM2 protein-protein interaction, Ph.D. thesis, University of East Anglia, 2016.

[3] D. P. Lane, Cancer. p53, guardian of the genome, Nature 358 (1992) 15–16.

[4] J. G. Teodoro, S. K. Evans, M. R. Green, Inhibition of tumor angiogenesis by p53: a new role for the guardian of the genome, Journal of molecular medicine 85 (2007) 1175–1186.

[5] T. Hamzehloie, M. Mojarrad, M. Hasanzadeh_Nazarabadi, S. Shekouhi, The role of tumor protein 53 mutations in common human cancers and

targeting the murine double minute 2–p53 interaction for cancer therapy, Iranian journal of medical sciences 37 (2012) 3.

[6] D. Liu, Y. Xu, p53, oxidative stress, and aging, Antioxidants & redox signaling 15 (2011) 1669–1678.

[7] S. Wang, Y. Zhao, D. Bernard, A. Aguilar, S. Kumar, Targeting the mdm2-p53 protein-protein interaction for new cancer therapeutics, in: Protein-protein interactions, Springer, 2012, pp. 57–79.

[8] G. L. Bond, W. Hu, A. J. Levine, Mdm2 is a central node in the p53 pathway: 12 years and counting, Current cancer drug targets 5 (2005) 3–8.

[9] D. Spiegelberg, A. C. Mortensen, S. Lundsten, C. J. Brown, D. P. Lane, M. Nestor, The mdm2/mdmx-p53 antagonist pm2 radiosensitizes wild-type p53 tumors, Cancer research 78 (2018) 5084–5093.

[10] L. T. Vassilev, B. T. Vu, B. Graves, D. Carvajal, F. Podlaski, Z. Filipovic, N. Kong, U. Kammlott, C. Lukacs, C. Klein, et al., In vivo activation of the p53 pathway by small-molecule antagonists of mdm2, Science 303 (2004) 844–848.

[11] K. Puszynski, A. Gandolfi, A. d'Onofrio, The pharmacodynamics of the p53-mdm2 targeting drug nutlin: the role of gene-switching noise, PLoS computational biology 10 (2014).

[12] L. G. De Pillis, A. Radunskaya, The dynamics of an optimally controlled tumor model: A case study, Mathematical and computer modelling 37 (2003) 1221–1244.

[13] M. Itik, M. U. Salamci, S. P. Banks, Optimal control of drug therapy in cancer treatment, Nonlinear Analysis: Theory, Methods & Applications 71 (2009) e1473–e1486.

[14] M. Itik, M. U. Salamci, S. P. Banks, Sdre optimal control of drug administration in cancer treatment, Turkish Journal of Electrical Engineering & Computer Sciences 18 (2010) 715–730.

[15] Y. Batmani, H. Khaloozadeh, Optimal chemotherapy in cancer treatment: state dependent riccati equation control and extended kalman filter, Optimal Control Applications and Methods 34 (2013) 562–577.

[16] N. Babaei, M. U. Salamci, Personalized drug administration for cancer treatment using model reference adaptive control, Journal of theoretical biology 371 (2015) 24–44.

[17] J. E. Purvis, K. W. Karhohs, C. Mock, E. Batchelor, A. Loewer, G. Lahav, p53 dynamics control cell fate, Science 336 (2012) 1440–1444.

[18] G. Lahav, N. Rosenfeld, A. Sigal, N. Geva-Zatorsky, A. J. Levine, M. B. Elowitz, U. Alon, Dynamics of the p53-mdm2 feedback loop in individual cells, Nature genetics 36 (2004) 147–150.

[19] T. Sun, J. Cui, Dynamics of p53 in response to dna damage: Mathematical modeling and perspective, Progress in biophysics and molecular biology 119 (2015) 175–182.

[20] E. A. Fedak, F. R. Adler, E. L. Young, L. M. Abegglen, J. D. Schiffman, Dynamics of the p53 response to ionizing and ultraviolet radiation, BioRxiv (2018) 367995.

[21] N. Geva-Zatorsky, N. Rosenfeld, S. Itzkovitz, R. Milo, A. Sigal, E. Dekel, T. Yarnitzky, Y. Liron, P. Polak, G. Lahav, et al., Oscillations and variability in the p53 system, Molecular systems biology 2 (2006).

[22] G. Tiana, M. Jensen, K. Sneppen, Time delay as a key to apoptosis induction in the p53 network, The European Physical Journal B-Condensed Matter and Complex Systems 29 (2002) 135–140.

[23] L. Ma, J. Wagner, J. J. Rice, W. Hu, A. J. Levine, G. A. Stolovitzky, A plausible model for the digital response of p53 to dna damage, Proceedings of the National Academy of Sciences 102 (2005) 14266–14271.

[24] J. Wagner, L. Ma, J. Rice, W. Hu, A. Levine, G. Stolovitzky, p53–mdm2 loop controlled by a balance of its feedback strength and effective dampening using atm and delayed feedback, IEE Proceedings-Systems Biology 152 (2005) 109–118.

[25] A. Ciliberto, B. Novák, J. J. Tyson, Steady states and oscillations in the p53/mdm2 network, Cell cycle 4 (2005) 488–493.

[26] E. Batchelor, C. S. Mock, I. Bhan, A. Loewer, G. Lahav, Recurrent initiation: a mechanism for triggering p53 pulses in response to dna damage, Molecular cell 30 (2008) 277–289.

[27] G. G. Rigatos, Non-linear feedback control of the p53 protein–mdm2 inhibitor system using the derivative-free non-linear kalman filter, IET systems biology 10 (2016) 94–106.

[28] M. Haseeb, S. Azam, A. Bhatti, R. Azam, M. Ullah, S. Fazal, On p53 revival using system oriented drug dosage design, Journal of theoretical biology 415 (2017) 53–57.

[29] M. R. Azam, S. Fazal, M. Ullah, A. I. Bhatti, System-based strategies for p53 recovery, IET systems biology 12 (2018) 101–107.

[30] M. R. Azam, V. I. Utkin, A. A. Uppal, A. I. Bhatti, Sliding mode controller–observer pair for p53 pathway, IET systems biology 13 (2019) 204–211.

[31] A. Hunziker, M. H. Jensen, S. Krishna, Stress-specific response of the p53-mdm2 feedback loop, BMC systems biology 4 (2010) 94.

[32] Y. Feng, F. Han, X. Yu, Chattering free full-order sliding-mode control, Automatica 50 (2014) 1310–1314.

[33] V. I. Utkin, Sliding modes in optimization and control problems, 1992.

[34] K. D. Young, V. I. Utkin, U. Ozguner, A control engineer's guide to sliding mode control, IEEE transactions on control systems technology 7 (1999) 328–342.

[35] X. Yu, O. Kaynak, Sliding-mode control with soft computing: A survey, IEEE Transactions on Industrial Electronics 56 (2009) 3275–3285.

[36] M. Ye, H. Wang, A robust adaptive chattering-free sliding mode control strategy for automotive electronic throttle system via genetic algorithm, IEEE Access 8 (2019) 68–80.

[37] Y. Hong, G. Yang, D. Cheng, S. Spurgeon, Finite time convergent control using terminal sliding mode, Journal of Control Theory and Applications 2 (2004) 69–74.

[38] C. Edwards, S. K. Spurgeon, On the development of discontinuous observers, International Journal of control 59 (1994) 1211–1229.

[39] A. A. Uppal, S. S. Butt, Q. Khan, H. Aschemann, Robust tracking of the heating value in an underground coal gasification process using dynamic integral sliding mode control and a gain-scheduled modified utkin observer, Journal of Process Control 73 (2019) 113–122.

[40] M. C. Teixeira, S. H. Zak, Stabilizing controller design for uncertain nonlinear systems using fuzzy models, IEEE Transactions on Fuzzy systems 7 (1999) 133–142.

[41] C. Edwards, S. Spurgeon, Sliding mode control: theory and applications, Crc Press, 1998.

[42] S. A. Qureshi, In vitro-in vivo correlation (ivivc) and determining drug concentrations in blood from dissolution testing–a simple and practical approach, The Open Drug Delivery Journal 4 (2010).

[43] A. Hunziker, M. H. Jensen, S. Krishna, Supplementary information for "stress-specific response of the p53-mdm2 feedback loop" (????).

[44] Y. V. Wang, M. Wade, E. Wong, Y.-C. Li, L. W. Rodewald, G. M. Wahl, Quantitative analyses reveal the importance of regulated hdmx degradation

for p53 activation, Proceedings of the National Academy of Sciences 104 (2007) 12365–12370.

[45] F. Zhang, M. Tagen, S. Throm, J. Mallari, L. Miller, R. K. Guy, M. A. Dyer, R. T. Williams, M. F. Roussel, K. Nemeth, et al., Whole-body physiologically based pharmacokinetic model for nutlin-3a in mice after intravenous and oral administration, Drug metabolism and disposition 39 (2011) 15–21.